

Turbulent Flow and Heat Transfer Problem in the Electromagnetic Continuous Casting Process

Theeradech Mookum, Benchawan Wiwatanapataphee, and Yong Hong Wu

Abstract—This paper aims to study the effect of turbulence on the flow of two fluids and the heat transfer - solidification process in electromagnetic continuous steel casting. The complete set of field equations is established. The flow pattern of the fluids, the meniscus shape and temperature field as well as solidification profiles obtained from the model with and with no turbulence effect are presented. The results show that the model with turbulence gives a large circulation zone above the jet, much larger variation of the meniscus geometry, a slow solidification rate and higher temperature in the top part of the strand region.

Keywords—Electromagnetic continuous steel casting process, turbulent flow, heat transfer, two-fluid flow, level set method.

I. INTRODUCTION

THE surface control of continuous steel casting products is important to steel quality. Over the last decade, the technologies used to control the quality of the continuous casting products have been proposed such as neural networks [23], fuzzy logic [24], optimization [27], and electromagnetic continuous casting process [10], [15]. The electromagnetic steel casting process is a relatively new effective heat extraction process in which molten steel is withdrawn at a specified speed. In comparison with the normal continuous casting process, the electromagnetic continuous casting process possesses many advantages such as improving the surface quality, controlling the flow pattern of liquid steel, and removing the inclusions and gas bubbles [16], [28].

Manuscript received April 7, 2011; revised May 30, 2011. This work was supported by the Office of the Higher Education Commission and the Thailand Research Fund through the Royal Golden Jubilee Ph.D. Program (Grant No. PHD/0212/2549), and an Australia Research Council Discovery project grant.

T. Mookum is with School of Science, Mae Fah Luang University, 333 Moo 1, Thasud, Muang, Chiang Rai 57100 THAILAND (e-mail:t.mookum@sci.mfu.ac.th).

B. Wiwatanapataphee is with Department of Mathematics, Faculty of Science, Mahidol University, 272 Rama 6 Road, Rajthevee, Bangkok 10400 THAILAND (corresponding author; e-mail:scbww@mahidol.ac.th).

Y.H. Wu is with Department of Mathematics and Statistics, Curtin University of Technology, Perth, WA 6845 AUSTRALIA (e-mail:yhwu@maths.curtin.edu.au).

Due to these advantages, great efforts have been made to develop this process over the last decade and the percentage of steel in the world produced by this process is increasing.

In the electromagnetic casting, a coil is mounted around the casting mould. The magnetic field generated from the source current through the coil induces the electric current in the steel pool. This current not only heats the molten steel but also generates an electromagnetic force in the molten steel. During the process, the molten steel is poured from a ladle into an intermediate container known as a tundish. The molten steel from the tundish is transferred through a submerged entry nozzle into a water-cooled mould, where intense cooling causes a thin solidified steel shell to form around the edge of the steel, leaving a large molten core inside the shell. To facilitate the process, mould powder or lubricant oil is added at the top of the mould to prevent the steel from oxidizing. The interface between the molten steel and lubricant oil is known as a “meniscus”. The mould is oscillated vertically and then the lubricant liquid is dragged into the gap between the solidified strand and the mould walls. This can prevent the steel from sticking to the solidifying shell. After leaving the mould, the solidified strand is supported by a set of rollers, cooled down by water sprays and then subsequently cooled through radiation. When the casting has attained the desired length, it is cut off with a cutter.

The electromagnetic field imposed to the process is the effective technology to control heat transport and solidification [2], [5], [20], [25], [26]. The electromagnetic force can reduce the molten steel flow from hitting the wall [7], [28] and push the meniscus away from the mould during casting [19], which reduces the surface contact between the melt and the wall. The behavior of electromagnetic stirring, fluid flow, heat transfer with solidification and oscillation marks on the steel surface is crucial to the quality and productivity of the process. The effect of the electromagnetic field on turbulent flow has also been investigated [8], [6], [22], [28].

With the limitation of experiments in the continuous casting process, mathematical models become an important tool to understand the physical phenom-

ena. Over the last few decades, most of the research efforts have been focussed on investigating the flow pattern and heat transfer problems in the continuous casting process [1], [4], [7], [9], [11], [18], [21]. Mookum [12], [13] presented a mathematical model to study the effect of electromagnetic field on the flow and temperature fields. The results indicated that the electromagnetic force reduced the speed of the molten steel near the mould wall. Wu and Wiwatanapataphee [29], [30] proposed a mathematical model to solve the coupled turbulent two-fluid flow and heat transfer with solidification. However, many phenomena such as the heat transfer process, the formation of oscillation marks and the meniscus behavior, have not been fully understood nor well controlled.

In this study, we extend the previous work [14] and propose a three-dimensional mathematical model for the problem of turbulent two-fluid flow and heat transfer with solidification in the electromagnetic continuous steel casting process. The effect of turbulent flow on temperature distribution and meniscus surface is investigated. The rest of the paper is organized as follows. In section two, a complete set of field equations and finite element formulation are given. Section three gives a numerical study to demonstrate the effect of electromagnetic force on the flow pattern, the heat transfer and solidification process as well as the meniscus shape.

II. MATHEMATICAL MODELS

A. Governing Equations

In this work, we study the effect of the electromagnetic force on the turbulent flow of fluids in the continuous steel casting process. In the mould region, there are two immiscible fluids, namely molten steel region (Ω_s) and lubricant oil region (Ω_o). To study the motion of the two fluids, we introduce the level set function ϕ as

$$\phi(x_i, t) = \begin{cases} 0 & \text{if } x_i \in \Omega_s \\ 0.5 & \text{if } x_i \in \Gamma_{int} \\ 1 & \text{if } x_i \in \Omega_o, \end{cases} \quad (1)$$

where Γ_{int} is the interface between the molten steel and the lubricant oil. Using ϕ , we can define the density, ρ , and the viscosity, μ , as follows:

$$\rho = \rho_s + (\rho_o - \rho_s)\phi, \quad (2)$$

$$\mu = \mu_s + (\mu_o - \mu_s)\phi, \quad (3)$$

where the subscripts s and o denote respectively the molten steel and lubricant oil.

The velocity and pressure fields described by the incompressible Navier-Stokes equations for the two-fluid flow are given below

$$\frac{\partial u_i}{\partial x_i} = 0, \quad (4)$$

$$\begin{aligned} \rho \left(\frac{\partial u_i}{\partial t} + u_j \frac{\partial u_i}{\partial x_j} \right) + \frac{\partial p}{\partial x_i} - \frac{\partial}{\partial x_j} \left(\mu_{eff} \left(\frac{\partial u_i}{\partial x_j} + \frac{\partial u_j}{\partial x_i} \right) \right) \\ = \rho g_i + F_{em_i} + F_{st_i} + F_i(u_i, x_i, t), \end{aligned} \quad (5)$$

where u_i represents the velocity of the fluids, p is the fluid pressure, g_i is the gravitational acceleration, F_{em_i} is the electromagnetic force, F_{st_i} is the surface tension force and F_i is the forcing function.

To solve equations (4) and (5), we need to couple the two-fluid flow problem with the heat transfer problem. Based on the enthalpy formulation, the temperature field is governed by the following equation:

$$\begin{aligned} \rho c \left(\frac{\partial T}{\partial t} + u_j \frac{\partial T}{\partial x_j} \right) = \frac{\partial}{\partial x_j} \left(k_{eff} \frac{\partial T}{\partial x_j} \right) \\ - \rho_s \left(\frac{\partial H_L}{\partial t} + u_j \frac{\partial H_L}{\partial x_j} \right) (1 - \phi), \end{aligned} \quad (6)$$

where T is the temperature, H_L is the latent heat defined as $H_L = Lf(T)$ in which L represents the latent heat of liquid steel. The liquid fraction $f(T)$ is given by

$$f(T) = \begin{cases} 0 & \text{if } T \leq T_S, \\ \frac{T - T_S}{T_L - T_S} & \text{if } T_S < T < T_L, \\ 1 & \text{if } T \geq T_L, \end{cases} \quad (7)$$

where T_S and T_L are the solidification temperature and melting temperature of the steel, respectively. The thermal conductivity, k , and the heat capacity, c , are expressed in terms of ϕ as follows:

$$k = k_s + (k_o - k_s)\phi, \quad (8)$$

$$c = c_s + (c_o - c_s)\phi. \quad (9)$$

The effective viscosity, μ_{eff} , and the effective thermal conductivity, k_{eff} , in equations (5) and (6), respectively, are given by

$$\mu_{eff} = \mu + \mu_t, \quad k_{eff} = k + \frac{c\mu_t}{\sigma_t}, \quad (10)$$

where σ_t is the turbulence Prandtl number assumed as 0.9 [1]. The turbulent viscosity, μ_t , is determined by

$$\mu_t = \rho C_\mu \frac{K^2}{\varepsilon}. \quad (11)$$

The coefficient C_μ is suggested to be 0.09 [9], K is the turbulent kinetic energy and ε is the turbulent

dissipation rate. The two-equation $K - \varepsilon$ model is used to study the effect of turbulence on the velocity and temperature fields, namely

$$\rho \left(\frac{\partial K}{\partial t} + u_j \frac{\partial K}{\partial x_j} \right) = \frac{\partial}{\partial x_j} \left[\left(\mu + \frac{\mu_t}{\sigma_K} \right) \frac{\partial K}{\partial x_j} \right] - \frac{\mu_t}{\sigma_t} \beta g_i \frac{\partial T}{\partial x_i} + \mu_t G - \rho \varepsilon \quad (12)$$

$$\rho \left(\frac{\partial \varepsilon}{\partial t} + u_j \frac{\partial \varepsilon}{\partial x_j} \right) = \frac{\partial}{\partial x_j} \left[\left(\mu + \frac{\mu_t}{\sigma_\varepsilon} \right) \frac{\partial \varepsilon}{\partial x_j} \right] + C_1(1 - C_3) \frac{\varepsilon \mu_t}{K \sigma_t} \beta g_i \frac{\partial T}{\partial x_i} + C_1 \varepsilon \frac{\mu_t}{K} G - C_2 \rho \frac{\varepsilon^2}{K} \quad (13)$$

where $G = \frac{\partial u_i}{\partial x_j} \left(\frac{\partial u_i}{\partial x_j} + \frac{\partial u_j}{\partial x_i} \right)$, β is the thermal expansion of steel, the coefficients $C_1 = 1.44$, $C_2 = 1.92$, $\sigma_K = 1$ and $\sigma_\varepsilon = 1.3$ [9].

To determine the movement of the interface, the level set function is obtained by solving the following equation [17]:

$$\frac{\partial \phi}{\partial t} + u_j \frac{\partial \phi}{\partial x_j} = \gamma \frac{\partial}{\partial x_j} \left(\epsilon \frac{\partial \phi}{\partial x_j} - \phi(1 - \phi) \hat{n}_j \right). \quad (14)$$

The quantities γ and ϵ are reinitialization parameter and thickness of the interface. The reinitialization of equation (14) is given by

$$\frac{\partial \phi}{\partial t} = \gamma \frac{\partial}{\partial x_j} \left(\epsilon \frac{\partial \phi}{\partial x_j} - \phi(1 - \phi) \hat{n}_j \right). \quad (15)$$

The equation (15) is first solved to obtain the initial condition for the level set equation (14).

Based on our previous work in [12], the electromagnetic force can be determined by

$$\mathbf{F}_{em} = \mathbf{J} \times (\nabla \times \mathbf{A}), \quad (16)$$

where \mathbf{J} and \mathbf{A} denote the total current density and the magnetic vector potential, respectively. To obtain the electromagnetic force, the magnetic vector potential \mathbf{A} and the scalar potential φ are determined from Maxwell's equations by

$$\nabla \cdot (-\eta \nabla \varphi + \mathbf{J}^s) = 0, \quad (17)$$

$$-\frac{1}{\nu} \nabla^2 \mathbf{A} + \eta \omega \mathbf{A} = -\eta \nabla \varphi + \mathbf{J}^s, \quad (18)$$

where \mathbf{J}^s is the source current density, η is the electric conductivity, ν is the magnetic permeability, ω is the current frequency, and $\iota = \sqrt{-1}$.

The surface tension force in equation (5) concentrated around the interface can be expressed as

$$\mathbf{F}_{st} = \sigma \kappa(\phi) \delta(\phi) \hat{\mathbf{n}}, \quad (19)$$

where σ , $\hat{\mathbf{n}}$, and κ are respectively the surface tension coefficient, the interface normal vector, and the interfacial curvature. The quantities $\hat{\mathbf{n}}$, and κ are calculated by $\hat{\mathbf{n}} = \frac{\nabla \phi}{|\nabla \phi|}$ and $\kappa(\phi) = -\nabla \cdot \hat{\mathbf{n}}$. The delta function $\delta(\phi)$ employed in this study is given by [3]

$$\delta(\phi) = 6|\nabla \phi| |\phi(1 - \phi)|. \quad (20)$$

The forcing function $\mathbf{F}(\mathbf{u}, \mathbf{x}, t)$ in equation (5) is determined, according to [1], by

$$\mathbf{F}(\mathbf{u}, \mathbf{x}, t) = C \frac{\mu_t (1 - f(T))^2}{f(T)^3} (\mathbf{u} - \mathbf{U}_{cast}), \quad (21)$$

where $\mathbf{U}_{cast} = (0, 0, U_{cast})$ in which U_{cast} represents the constant downward casting speed and C is the morphology constant.

To completely define the problem, a set of boundary conditions have been established to supplement the above field equations and are shown in Fig. 2.

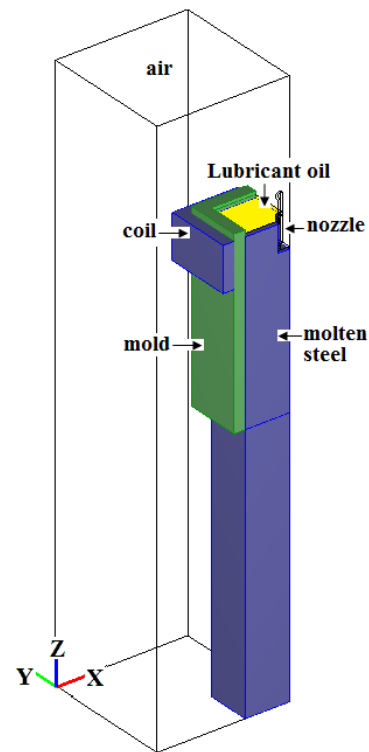


Fig. 1. Computation domain

B. Finite Element Formulation

In this study, we employ a Bubnov-Galerkin finite element method for the numerical simulation and investigation. The electromagnetic force in equation (16) is obtained first by solving the electromagnetic field in equations (17) and (18). In order to obtain

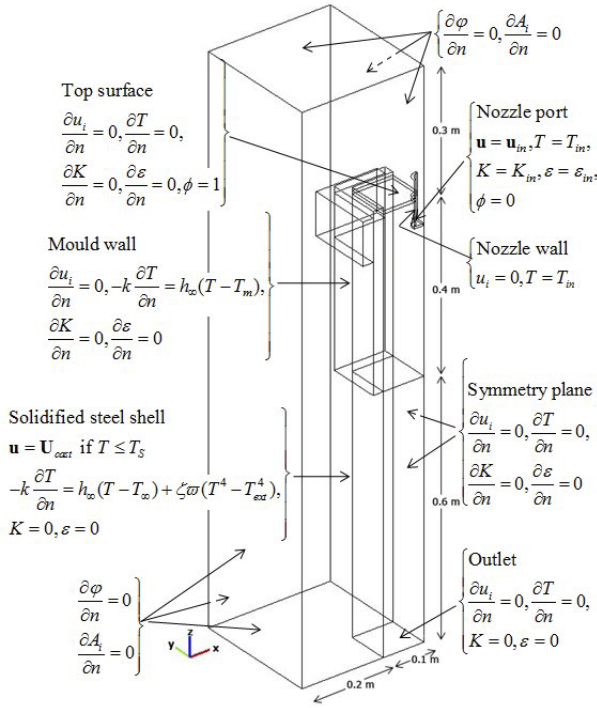


Fig. 2. Boundary conditions

the finite element solution of A_i and φ , the variational problem for the equations (17) and (18) are established:

Find $\varphi, A_i \in H^1(\Omega)$ such that for all test functions $w^b, w_i^c \in H_0^1(\Omega)$, the relevant Dirichlet type boundary conditions are satisfied and

$$\int_{\Omega} w^b \frac{\partial}{\partial x_j} \left(-\eta \frac{\partial \varphi}{\partial x_j} + J_j^s \right) d\Omega = 0, \quad (22)$$

$$\begin{aligned} & - \int_{\Omega} w_i^c \frac{1}{\nu} \frac{\partial^2 A_i}{\partial x_j \partial x_j} d\Omega + \int_{\Omega} w_i^c \eta \omega A_i d\Omega \\ & = \int_{\Omega} w_i^c \left(-\eta \frac{\partial \varphi}{\partial x_i} + J_i^s \right) d\Omega, \end{aligned} \quad (23)$$

where $H^1(\Omega)$ is the Sobolev space $W^{1,2}(\Omega)$ with norm $\| \cdot \|_{1,2,\Omega}$, $H_0^1(\Omega) = \{v \in H^1(\Omega) | v = 0 \text{ on the boundary}\}$. By using the Galerkin finite element formulation, we obtain the following discretization system

$$\eta M \tilde{\varphi} = \mathbf{F}_J, \quad (24)$$

$$\left(\frac{1}{\nu} M + \eta \omega B \right) \tilde{A} = \mathbf{F}_A, \quad (25)$$

where M and B are the coefficient matrices. To solve the steady state system of equations (24) and (25), we can solve first equation (24) for $\tilde{\varphi}$ and then use this solution to solve equation (25) for \tilde{A} .

For the finite element solution of u_i, p, T, ϕ, K and ε , the variational statement for the boundary

value problem corresponding to the the equations (4), (5), (6), (12), (13), and (14) subjected to relevant boundary conditions is established as follows:

Find $u_i, p, T, \phi, K, \varepsilon \in H^1(\Omega)$ such that for all $w^i, w^p, w^\tau, w^\phi, w^K, w^\varepsilon \in H_0^1(\Omega)$, all relevant Dirichlet type boundary conditions are satisfied and

$$\int_{\Omega} w^p \frac{\partial u_j}{\partial x_j} d\Omega = 0, \quad (26)$$

$$\begin{aligned} & \int_{\Omega} w^i \frac{\partial u_i}{\partial t} d\Omega + \int_{\Omega} w_i (u_j \frac{\partial u_i}{\partial x_j}) d\Omega \\ & - \int_{\Omega} \frac{1}{\rho} \frac{\partial w^i}{\partial x_i} p d\Omega + \int_{\Omega} \frac{\mu}{\rho} \left(\frac{\partial w^i}{\partial x_j} \frac{\partial u_i}{\partial x_j} + \frac{\partial w^i}{\partial x_i} \frac{\partial u_j}{\partial x_i} \right) d\Omega \\ & = \int_{\Omega} w^i g_i d\Omega + \int_{\Omega} \frac{1}{\rho} w^i F_{em_i} d\Omega \\ & + \int_{\Omega} \frac{1}{\rho} w^i F_{st_i} d\Omega + \int_{\Gamma_{wall}} \frac{\mu}{\rho h} w^i u_i d\Gamma, \end{aligned} \quad (27)$$

$$\begin{aligned} & \int_{\Omega} w^\tau \frac{\partial T}{\partial t} d\Omega + \int_{\Omega} w^\tau (u_j \frac{\partial T}{\partial x_j}) d\Omega \\ & + \int_{\Omega} \frac{k}{\rho c} \frac{\partial w^\tau}{\partial x_j} \frac{\partial T}{\partial x_j} d\Omega = - \int_{\Gamma_{wall}} \frac{1}{\rho c} w^\tau h_\infty (T - T_m) d\Gamma \\ & - \int_{\Gamma_{strand}} \frac{1}{\rho c} w^\tau (h_\infty (T - T_\infty) + \zeta \omega (T^4 - T_{ext}^4)) d\Gamma \\ & - \int_{\Omega} \frac{1}{c_s} w^\tau \left(\frac{\partial H_L}{\partial t} + (u_j \frac{\partial H_L}{\partial x_j}) \right) (1 - \phi) d\Omega, \end{aligned} \quad (28)$$

$$\begin{aligned} & \int_{\Omega} w^\phi \frac{\partial \phi}{\partial t} d\Omega + \int_{\Omega} w^\phi (u_j \frac{\partial \phi}{\partial x_j}) d\Omega \\ & = \int_{\Omega} w^\phi \gamma \frac{\partial}{\partial x_j} \left(\varepsilon \frac{\partial \phi}{\partial x_j} - \phi (1 - \phi) \hat{n}_j \right) d\Omega. \end{aligned} \quad (29)$$

$$\begin{aligned} & \int_{\Omega} w^K \rho \frac{\partial K}{\partial t} d\Omega + \int_{\Omega} w^K u_j \frac{\partial K}{\partial x_j} d\Omega \\ & = \int_{\Omega} w^K \frac{\partial}{\partial x_j} \left[\left(\mu + \frac{\mu_t}{\sigma_K} \right) \frac{\partial K}{\partial x_j} \right] d\Omega \\ & - \int_{\Omega} w^K \frac{\mu_t}{\sigma_t} \beta g_i \frac{\partial T}{\partial x_i} d\Omega + \int_{\Omega} w^K \mu_t G d\Omega \\ & - \int_{\Omega} w^K \rho \varepsilon d\Omega \end{aligned} \quad (30)$$

$$\begin{aligned} & \int_{\Omega} w^\varepsilon \rho \frac{\partial \varepsilon}{\partial t} d\Omega + \int_{\Omega} w^\varepsilon u_j \frac{\partial \varepsilon}{\partial x_j} d\Omega \\ & = \int_{\Omega} w^\varepsilon \frac{\partial}{\partial x_j} \left[\left(\mu + \frac{\mu_t}{\sigma_\varepsilon} \right) \frac{\partial \varepsilon}{\partial x_j} \right] d\Omega \\ & + \int_{\Omega} w^\varepsilon C_1 (1 - C_3) \frac{\varepsilon \mu_t}{K \sigma_t} \beta g_i \frac{\partial T}{\partial x_i} d\Omega \\ & + \int_{\Omega} w^\varepsilon C_1 \varepsilon \frac{\mu_t}{K} G d\Omega - \int_{\Omega} w^\varepsilon C_2 \rho \frac{\varepsilon^2}{K} d\Omega \end{aligned} \quad (31)$$

The above equations for $(u_x, u_y, u_z, p, T, \phi, K, \varepsilon)$ are then discretized in space by the level set finite element method to yield the following system of nonlinear ordinary differential equations

$$\bar{M}\dot{\mathbf{U}} + \bar{B}\mathbf{U} = \bar{\mathbf{F}}, \quad (32)$$

where $\mathbf{U} = \{u_{xi}, u_{yi}, u_{zi}, p_i, T_i, K_i, \varepsilon_i\}_{i=1}^N$ are the value of $u_x, u_y, u_z, p, T, \phi, K$, and ε at the nodes of the finite element mesh. The coefficient matrix \bar{M} corresponds to the transient terms in the governing partial differential equations, the matrix \bar{B} corresponds to the advection and diffusion terms, and the vector $\bar{\mathbf{F}}$ corresponds to the external body force.

To solve the system of ordinary differential equations (32), the backward Euler scheme is employed. The convergence criteria used for the iterative scheme is given by

$$\|\mathbf{R}_n^{i+1} - \mathbf{R}_n^i\| < Tol, \quad (33)$$

where $i + 1$ and i denote the iterative computation steps, R_n represents the unknown vector of the n th variable on the finite element nodes, $\|\cdot\|$ denotes the Euclidean norm and Tol is a very small positive number.

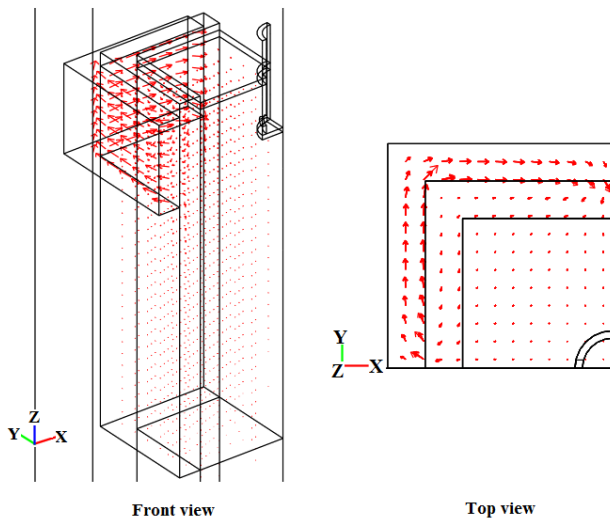


Fig. 3. Vector plot of the total current density on the front and top view

III. NUMERICAL RESULTS

For numerical investigation, we consider a square billet with a width of 0.2 m and a depth of 0.4 m , and a submerged entry nozzle with port angle of 12° downward. The inlet velocity of molten steel is 0.12 m/s ; the molten steel is assumed to have 5°C of

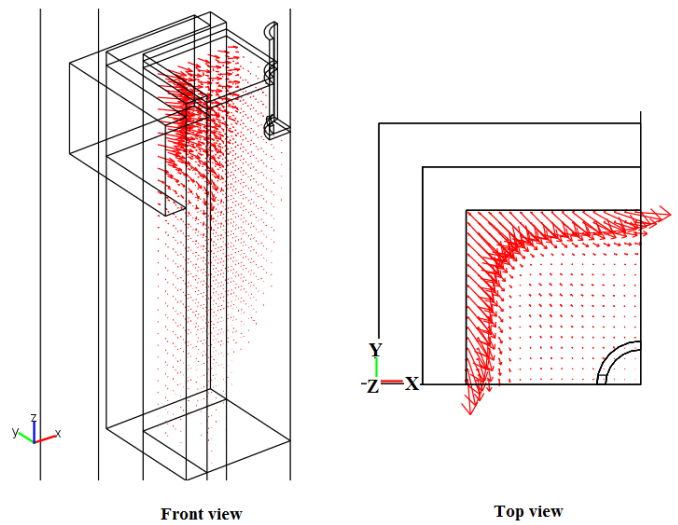


Fig. 4. Vector plot of the electromagnetic force on the front and top view

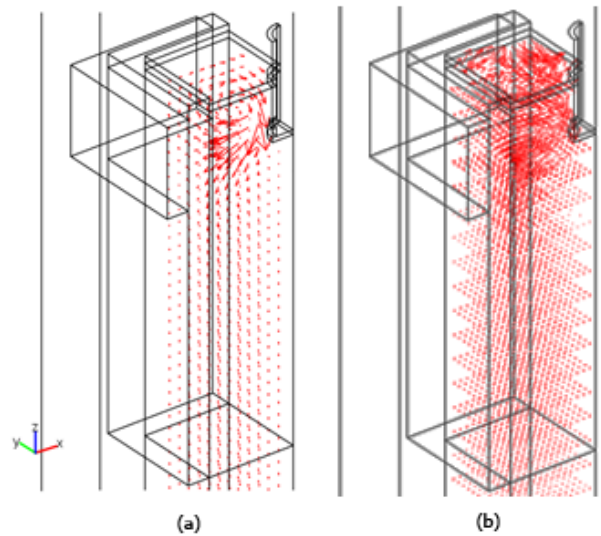


Fig. 5. The velocity fields under two different cases: (a) with turbulence effect;(b) with no turbulence effect

super-heat; and the delivery turbulent kinetic energy and its dissipation rate are respectively $0.0502\text{ m}^2/\text{s}^2$ and $0.457\text{ m}^2/\text{s}^2$. The values of other parameters are given in Table I. The computation domain shown in Fig. 1 represents one quadrant of the casting steel system consisting of the strand region occupied by the steel and lubricant oil on the top, the mould region, the coil region, and the environment region. The domain is discretized using 60,462 tetrahedral elements with a total of 625,737 degrees of freedom.

Fig. 3 shows the total current density \mathbf{J} on the front and top views. The result shows that the current density concentrated around the edge of the mould

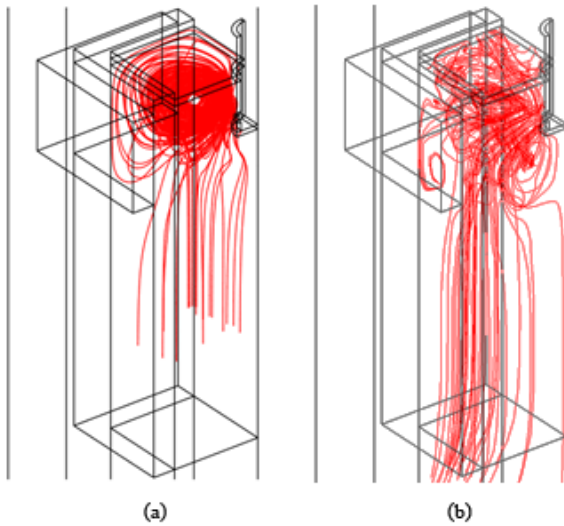


Fig. 6. The streamlines of the molten steel under two different cases: (a) with turbulence effect; (b) with no turbulence effect

TABLE I
PARAMETERS USED IN NUMERICAL SIMULATION

Parameters	Value
ν	$4\pi \times 10^{-7}$ Henry/m
η	4.032×10^6 $\Omega^{-1}m^{-1}$
ω	320 Hz
U_{cast}	-0.000575 m/s
ρ_s	7800 kg/m ³
ρ_o	2728 kg/m ³
μ_s	0.001 Pa·s
μ_o	0.0214 Pa·s
σ	1.6 m/s ²
ϵ	0.001 m
g	-9.8 m/s ²
T_{in}	1535 °C
T_L	1525 °C
T_S	1465 °C
T_∞	150 °C
T_{ext}	100 °C
T_m	1400 °C
c_s	465 J/kg °C
c_o	1000 J/kg °C
k_s	35 W/m °C
k_o	1 W/m °C
L	2.72×10^5 J/kg
C	1.8×10^6 m ⁻²
h_∞	1079 W/m ² °C
β	0.00003 °C ⁻¹
ϖ	0.4
ς	5.66×10^{-8} W/m ² K ⁴

wall. The directions are basically in the clockwise direction parallel to the horizontal plane. Fig. 4 shows the electromagnetic forces \mathbf{F}_{em} acting on the molten steel, which are basically in the horizontal direction toward the central line and concentrate near the surface of steel pool.

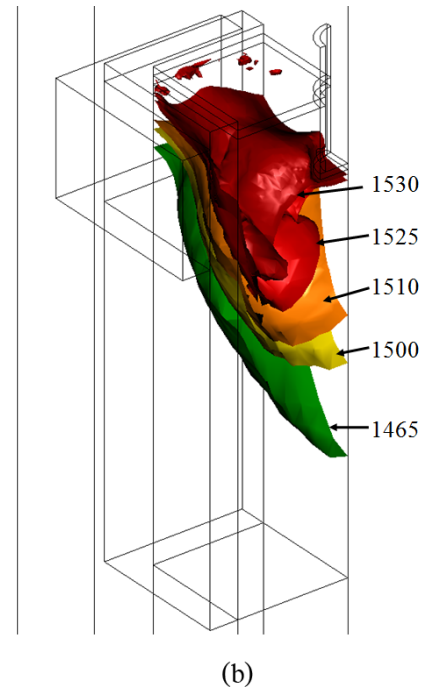


Fig. 7. The temperature profiles of the steel strand under two different cases: (a) with turbulence effect; (b) with no turbulence effect

To investigate the influence of turbulence effect, velocity field, temperature distribution in the top part of the strand region and the meniscus shape obtained from the models with and with no turbulence effect are analyzed. It can be seen on Figs. 5, 6, 7 and 8 that turbulence has significant effect on the velocity field, the streamlines, the temperature field of the molten

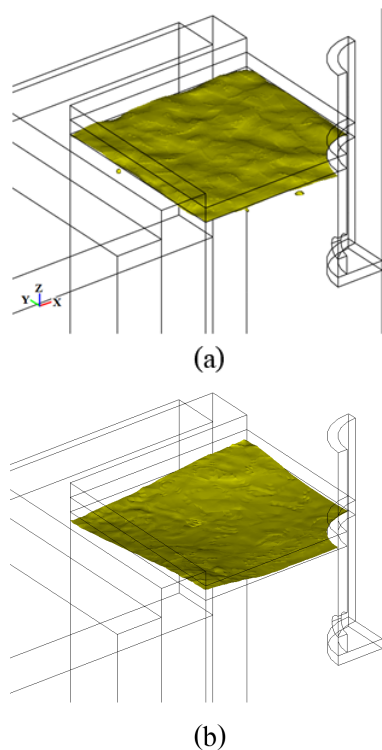


Fig. 8. The shape of the meniscus surface between the lubricant oil and the molten steel under two different cases: (a) with turbulence effect; (b) with no turbulence effect

steel, and the meniscus shape between the two fluids. The results show that under the turbulence condition, A large circulation zone presents above the jet as shown in Figs. 5(a) and 6(a), and molten steel starts to solidify at the bottom of the coil as shown in Fig.7(a). In the model with no turbulence effect, two recirculation zones above and below the jet appear as shown in Figs. 5(b) and 6(b), and molten steel starts to solidified ($T = 1465$) at the top of the coil as shown in Fig. 7(a). The meniscus shape enlarged by flow is different as shown in Figs. 8(a-b). In the model with no turbulence effect, meniscus shape is concave along the mould wall and convex along the symmetry plane. In the model with turbulence effect, the meniscus shape varies significantly in the liquid pool from the center to the edge of the steel strand.

IV. CONCLUDING REMARKS

A three-dimensional mathematical model has been developed to study the coupled turbulent two-fluid flow and heat transfer process in electromagnetic continuous steel casting. Turbulence effect on the velocity field, temperature field, and meniscus shape has been investigated. The results show that turbulence has significant effect on the velocity field, streamlines, temperature field of the molten steel and the meniscus shape between the two fluids. In

the model with no turbulence effect, there are two recirculation zones respectively above and below the jet, and initial solidification of molten steel occurs at the top of the coil, and the concave and convex shape of the meniscus appears along the mould wall and convex along the symmetry plane, respectively. On the other hand, the model with turbulence gives a large circulation zone above the jet, a slow solidification rate, and a large variation of the meniscus shape. It can be concluded that the model with turbulence gives much larger variation of the meniscus geometry and higher temperature in the top part of the strand region.

ACKNOWLEDGMENT

The authors gratefully acknowledge the support of the Office of the Higher Education Commission and the Thailand Research Fund through the Royal Golden Jubilee Ph.D. Program (Grant No. PHD/0212/2549), and an Australia Research Council Discovery project grant.

REFERENCES

- [1] M.R. Aboutalebi, M. Hasan, and R.I.I. Guthrie, Coupled turbulent flow, heat and solute transport in continuous casting processes, *Metall. Mater. Trans.* vol.26B, 1995, pp. 731-744.
- [2] P.R. Cha, Y.H. Hwang, H.S. Nam, S.H. Chung, and J.K. Yoon, 3D numerical analysis on electromagnetic and fluid dynamic phenomena in a soft contact electromagnetic slab caster, *ISIJ Inter.* vol.38, 1998, pp. 403-410.
- [3] J.P.A. Bastos, and N. Sadowski, *Comsol multiphysics modeling guide version 3.4*, COMSOLAB 2007.
- [4] J.H. Ferziger, Simulation of incompressible turbulent flow, *Comput. Phys.* vol.69, 1987, pp. 1-48.
- [5] K. Fujisaki, In-mold electromagnetic stirring in continuous casting, *IEEE Trans. Industry Applications* vol.37, No.4, 2001, pp. 1098-1104.
- [6] M.Y. Ha, H.G. Lee, and S.H. Seong, Numerical simulation of three-dimensional flow, heat transfer, and solidification of steel in continuous casting mold with electromagnetic brake, *Metal. Mater. Inter.* vol.133, 2003, pp. 322-339.
- [7] K.G. Kang, H.S. Ryou, and N.K. Hur, Coupled turbulent flow, heat, and solute transport in continuous casting process with an electromagnetic brake, *Numer. Heat Trans. A.* vol.48, 2005, pp. 461-481.
- [8] D.S. Kim, W.S. Kim, and K.H. Cho, Numerical simulation of the coupled turbulent flow and macroscopic solidification in continuous casting with electromagnetic brake, *ISIJ. Inter.* vol.40, 2000, pp. 670-676.
- [9] B.E. Launder and D.B. Spalding, The numerical computation of turbulent flows, *Comput. Meth. Appl. Mech.* vol.3, 1974, pp. 269-289.
- [10] T.J. Li, K. Sassa, and S. Asai, Surface quality improvement of continuously cast metals by imposing intermittent high frequency magnetic field and synchronising the field with mold oscillation, *ISIJ. Inter.* vol.36, No.4, 1996, pp. 410-416.
- [11] P.R. Lopez, R.D. Morales, R.S. Perez, and L.G. Demedices, Structure of turbulent flow in slab mold, *Metall. Mater. Trans. B.* vol.36B, 2005, pp. 787-800.

- [12] T. Mookum, B. Wiwatanapataphee, and Y.H. Wu, Numerical simulation of three-dimensional fluid flow and heat transfer in electromagnetic steel casting, *Int. J. Pure. Appl. Math* vol.52, No.3, 2009, pp. 373-390.
- [13] T. Mookum, B. Wiwatanapataphee, and Y.H. Wu, Modeling of two-fluid flow and heat transfer with solidification in continuous steel casting process under electromagnetic force, *Int. J. Pure. Appl. Math* vol.63, No.2, 2009, pp. 183-195.
- [14] T. Mookum, B. Wiwatanapataphee, and Y.H. Wu, The effect of turbulence on two-fluid flow and heat transfer in continuous steel casting process, *Proceedings of the 4th WSEAS Int. Conf. on F-and-B'11*. ISBN:978-960-474-298-1, 2011, pp. 53-58.
- [15] H. Nakata, T. Inoue, H. Mori, K. Ayata, T. Murakami, and T. Kominami, Improvement of billet surface quality by ultra-high frequency electromagnetic casting, *ISIJ. Inter.* vol.42, 2002, pp. 246-272.
- [16] T.T. Natarajan and N. El-Kaddah, Finite element analysis of electromagnetic and fluid flow phenomena in rotary electromagnetic stirring of steel, *Appl. Math. Model.* vol.28, 2004, pp. 47-61.
- [17] E. Olssen, G. Kreiss, and S. Zahedi, A conservative level set method for two phase flow II, *J. Comput. Phys.* Vol.225, 2007, pp. 785-807.
- [18] R. Sánchez-Perez, R.D. Morales, M. Díaz-Cruz, O. Olivares-Xometl, and J. Palafox-Ramos, A physical model for the two-phase flow in a noncontinuous casting mold, *ISIJ. Inter.* vol.32, 1992, pp. 521-528.
- [19] K. Takatani, K. Nakai, N. Kasai, T. Watanabe, and H. Nakajima, Analysis of heat transfer and fluid flow in the continuous casting mold with electromagnetic brake, *ISIJ Inter.* vol.29, 1989, pp. 1063-1068.
- [20] G.R. Tallback and J.D. Lavers, Influence of model parameters on 3-D turbulent flow in an electromagnetic stirring system for continuous billet casting, *IEEE Trans. Magnetics* vol.40, No.2, 2004, pp. 597-600.
- [21] B.G. Thomas, Continuous casting: complex models, *Encyclopedia of Materials: Science and Technology* vol.2, 2001, pp. 1599-1609.
- [22] X.Y. Tian, F. Zou, B.W. Li, and J.C. He, Numerical analysis of coupled fluid flow, heat transfer and macroscopic solidification in the thin slab funnel shape mold with a new type EMBr, *Metall. Mater. Tran. B.* vol.41B, 2009, pp. 112-120.
- [23] G.O. Tirian and C. Pinca-Bretotean, Applications of neural networks in continuous casting, *WSEAS Trans. Sys.* Vol.8, No.6, 2009, pp. 693-702.
- [24] G.O. Tirian, C. Pinca-Bretotean, D. Cristea, and M. Topor, Applications of fuzzy logic in continuous casting, *WSEAS Trans. Sys. Contr.* Vol.5, No.3, 2010, pp. 133-142.
- [25] T. Toh, E. Takeuchi, M. Hojo, H. Kawai, S. Matsumura, Electromagnetic control of initial solidification in continuous casting of steel by low frequency alternating magnetic field. *ISIJ Inter.* vol.37, 1997, pp. 1112-1119.
- [26] L.B. Trindade, A.C.F. Vilela, A.F.F. Filho, M.T.M.B. Vilhena, and R.B. Soares, Numerical model of electromagnetic stirring for continuous casting billets, *IEEE Trans. Magnetics* vol.38, No.6, 2002, pp. 3658-3660.
- [27] M. Tufoi, I. Vela, C. Marta, D. Amariei, A.I. Tuta, and C. Mituletu, Optimization of withdrawing cylinder at vertical continuous casting of steel using CAD and CAE, *Int. J. Mech.* vol.5, No.1, 2011, pp. 10-18.
- [28] Y.H. Wu and B. Wiwatanapataphee, Modelling of turbulent flow and multi-phase heat transfer under electromagnetic force, *Disc. Cont. Dyn. Sys. B.* vol.8, 2007, pp. 695-706.
- [29] Y.H. Wu and B. Wiwatanapataphee, An enthalpy control volume method for transient mass and heat transport with solidification, *Int. J. Comput. Flu. Dyn* vol.18, 2004, pp. 577-584.
- [30] B. Wiwatanapataphee, Y.H. Wu, J. Archapitak, P.F. Siew and B. Unyong, A numerical study of the turbulent flow of molten steel in a domain with a phase-change boundary, *J. Comp. App. Math.* vol.166, 2004, pp. 307-319.